Role of deep sea temperature in the carbon cycle during the last glacial

Pamela Martin and David Archer
Department of Geophysical Sciences, University of Chicago, Chicago, Illinois, USA

David W. Lea
Department of Geological Sciences and the Marine Sciences Institute, University of California, Santa Barbara, California, USA

Received 20 April 2003; revised 24 May 2004; accepted 19 August 2004; published 18 June 2005.

[1] To characterize the response of Earth's climate system to increases in atmospheric CO_2, climate modelers define climate sensitivity as the change in global mean temperature in response to prescribed forcing. Here we turn this approach around and use estimates of ocean temperature change to investigate the mechanisms driving CO_2 variations over the last glacial. New records provide evidence of a link between deep ocean temperature and atmospheric CO_2 over the last glacial cycle. Two mechanisms simultaneously couple pCO_2 and deep ocean temperature: the temperature-dependent solubility of CO_2 in seawater and the atmospheric CO_2-dependent radiative forcing of temperature. Each of these forcing mechanisms leaves a unique slope of covariation between CO_2 and deep ocean temperature, which we estimate using numerical models of climate and the carbon cycle. The pCO_2/T slopes derived from paleoclimate data differ between the deglaciation and shorter 5-kyr duration events in marine isotope stage 3 (MIS 3), revealing different mechanisms driving atmospheric CO_2 variability. The amplitude of changes over the deglaciation coincides with estimates for CO_2 forcing of temperature; however, CO_2 changes during MIS 3 can be explained solely by temperature-dependent solubility driving variations in atmospheric pCO_2. The deep water temperature changes during MIS 3 may reflect changes in the temperature or relative contribution of Antarctic Bottom Water and play a role in the "bipolar seesaw."

Citation: Martin, P., D. Archer, and D. W. Lea (2005), Role of deep sea temperature in the carbon cycle during the last glacial, *Paleoceanography*, *20*, PA2015, doi:10.1029/2003PA000914.

1. Introduction

[2] Two factors relate atmospheric CO_2 and the temperature of the ocean. The first is the solubility of CO_2 gas in sea water, which increases with decreasing temperature, and the second is the radiative, or greenhouse, forcing of the temperature of Earth as a function of the concentration of CO_2 in the atmosphere. These two constraints in the climate system, CO_2 solubility and radiative equilibrium, are not independent and must be satisfied simultaneously. Their interaction can be visualized as lines on a plot of CO_2 and ocean T (Figure 1). Following an arbitrary perturbation to either component of the climate system, feedbacks governed by solubility and radiative equilibrium will cause a series of changes to both CO_2 and mean ocean temperature. The CO_2 concentration will relax toward solubility equilibrium (vertically on the plot) and ocean temperature will be forced toward radiative equilibrium (horizontally). For example, a slight increase in atmospheric CO_2 will warm the ocean, which will lead to a small increase in CO_2 due to outgassing, which in turn leads to additional warming. If the slope of the radiative equilibrium relation is steeper than that of the solubility relation, as model results described below predict, then the resulting trajectory will take atmospheric CO_2 and deep sea temperature to the intersection of the two lines (Figure 1a). This will occur on the 10^3-year timescale for heat and CO_2 to invade the deep sea.

[3] Much of the speculation about glacial/interglacial pCO_2 cycles has centered on ways of changing the distribution of CO_2 between the atmosphere and the ocean, independent of mean ocean temperature changes. Mechanisms include the biological pump, which exports carbon from surface waters to depth in the form of sinking particles [*Volk and Hoffert*, 1985], and the $CaCO_3$ cycle, which determines ocean pH [*Archer and Maier-Reimer*, 1994; *Berger*, 1978]. By forcing CO_2 independently of T, these scenarios displace the solubility relation vertically (Figure 1b). Vertical displacement of the solubility line moves the stable intersection between solubility and radiative equilibrium (the point to which the system relaxes), amplifying the primary CO_2 forcing. The signature of CO_2 forcing in climate records would be the temporal covariation of atmospheric CO_2 and deep water T quantitatively following the radiative relation.

[4] Alternatively, variations in mean ocean temperature can drive atmospheric pCO_2 by the solubility mechanism. Examples of temperature-forcing mechanisms include heat transport in the North Atlantic [*Stocker et al.*, 1992a], the albedo effect of continental ice sheets [*Manabe and Broccoli*, 1985], and direct orbital forcing [*Milankovitch*, 1930]. The effect would be to move the radiative relation horizontally (Figure 1c). As above, atmospheric pCO_2 and deep ocean T would relax to the new intersection of the two constraints,

0883-8305/05/2003PA000914

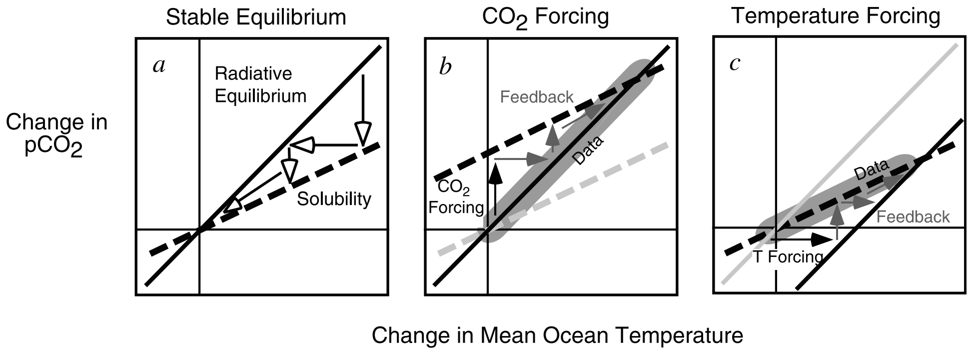

Figure 1. Schematic of the interplay between the solubility and the radiative CO_2 relations. (a) Solubility relation (dashed line) and radiative relation (solid line). The CO_2 concentration tends to relax vertically toward the solubility relation when forced by changing T, whereas T, forced radiatively by CO_2, relaxes horizontally toward the radiative line. Coupled together, the system relaxes toward the intersection of the two relations (open-headed arrows). (b) Effect of CO_2 forcing, such as changing the biological pump or the pH of the ocean. As the system relaxes to the new intersection between solubility and radiative relations, the original CO_2 forcing is amplified. Paleo-CO_2 and deep ocean temperature data would covary along the radiative relation (gray stippled region). (c) Effect of forcing the deep sea temperature, as by changing the circulation in the North Atlantic. The original temperature forcing is amplified by the changing solubility of CO_2. Paleodata would fall along the solubility relation (stippled region).

and as above, this dynamic amplifies the original temperature forcing. Temperature forcing would generate a record of pCO_2 and T variation that falls along the solubility relation. The amplitude of the feedback to either type of forcing depends on the relative slopes of the two relations; if they nearly coincide the feedback becomes larger.

[5] In this paper, we compare estimates of deep sea temperature change over the last 90 kyr with records of CO_2 from Antarctic ice cores and results from numerical models to investigate the mechanisms forcing CO_2 over the last glacial cycle.

2. Methods

[6] We base our analysis on reconstructions of deep sea temperature using the Mg/Ca ratio of benthic foraminifera and various estimates of glacial-interglacial deep sea temperature derived from foraminiferal $\delta^{18}O$ [*Adkins and Schrag*, 2001; *Chappell*, 2002; *Chappell and Shackleton*, 1986; *Labeyrie et al.*, 1987; *Schrag et al.*, 1996; *Shackleton*, 2000]. Mg/Ca is a direct recorder of temperature based on an empirical relationship between water temperature and shell Mg/Ca, which increases exponentially with increasing temperature [*Lear et al.*, 2000; *Martin et al.*, 2002b; *Rosenthal et al.*, 2000]. Foraminiferal $\delta^{18}O$ records changes in both temperature and $\delta^{18}O_{water}$ and the two signals must be separated to estimate temperature. The general approach to separating the signals has been to estimate glacial/interglacial changes in $\delta^{18}O_{water}$ (predominately an ice volume signal in deep waters) and assign the residual change in foraminiferal $\delta^{18}O$ to temperature. Methods used to characterize $\delta^{18}O_{water}$ include quantifying site to site differences in foraminiferal $\delta^{18}O$, estimating changes in sea level from coral terraces, and measuring pore water $\delta^{18}O$ [*Adkins and Schrag*, 2001; *Chappell*, 2002; *Chappell and Shackleton*, 1986; *Labeyrie et al.*, 1987; *Schrag et al.*, 1996; *Shackleton*, 2000].

[7] We examined Mg/Ca variation in the benthic foraminifera *Uvigerina sp*. in two deep sea cores in the eastern tropical Pacific. Because the deep Pacific dominates the ocean by volume, changes in deep water temperature in this region should be reflective of mean ocean changes. Martin et al. presented a ~250-kyr Mg-derived temperature record from deep eastern tropical Pacific core TR163-31P (3°35′S 83°57′ W; 3205 m) [*Martin et al.*, 2002b]. We augment this record with a second Mg-derived temperature record for the deglaciation from nearby core TR163-20B (3°30′N 90°47′ W; 3200 m). Depths in core TR163-31P were converted to age using a revised age-depth model constructed by comparison of the benthic oxygen isotope records from TR163-31P to the orbitally tuned oxygen isotope record from V19-30. The age model for TR163-20B was derived by comparison to TR163-31P (see supplementary data for both age models).[1] Samples were prepared following the full trace metal cleaning protocol [*Boyle and Keigwin*, 1985] which has been tested for minor elements [*Martin and Lea*, 2002] and analyzed by ICP-MS for Mg/Ca following the procedure in the work of *Martin et al.* [2002b]. Precision is estimated to be better than 3%. Benthic $\delta^{18}O$ data for core TR163-20B were generated in J. Kennett's laboratory at the University of California, Santa Barbara following standard protocol. New data are archived in Table 1.

[8] We have estimated temperature changes from Mg/Ca using the equation derived from core top data and the downcore response of *Uvigerina sp*. Measurements of the benthic foraminifera *Cibicidoides sp*. from a global assortment of core tops show an eleven percent increase in shell Mg/Ca per °C increase in temperature (Mg/Ca_{Cib} = 0.85e0.11*T). Downcore comparison of *C. wuellerstorfi* with coincident *Uvigerina sp*., a second genus of benthic foraminifera, in a

[1] Auxiliary material is available at ftp://ftp.agu.org/apend/pa/2003PA000914.

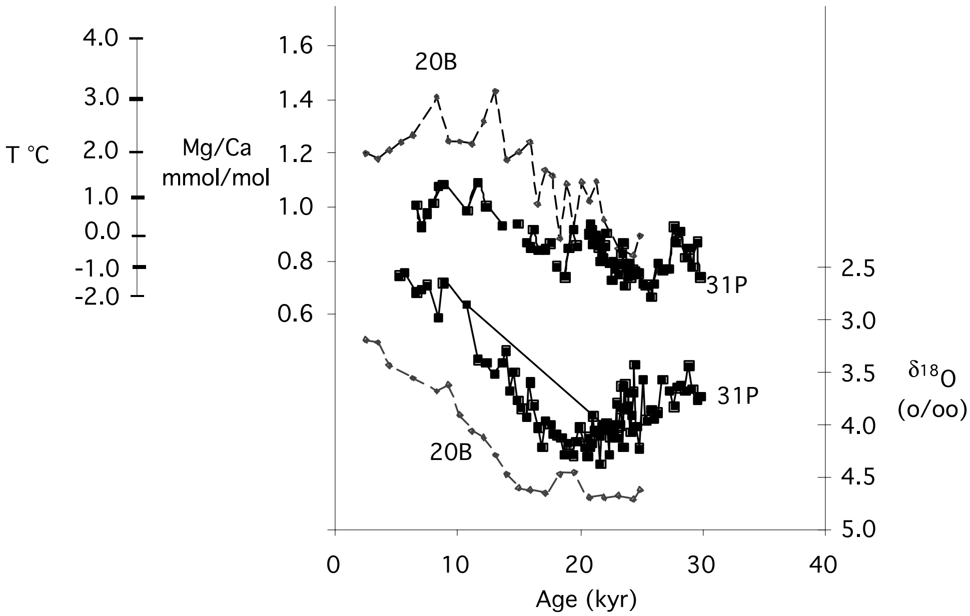

Figure 2. Mg/Ca, Mg-derived temperatures, and $\delta^{18}O$ in cores TR163-31P and TR163-20B. The black solid lines and squares represent data from core TR163-31P. The gray dashed lines and triangles represent data from core TR163-20B. Temperature estimates are derived using the empirically derived equation for Uvigerina sp.: Mg/Ca = 0.87exp(0.15*T). Data from TR163-31P were previously published in the work of *Martin et al.* [2002b].

deep tropical Atlantic core implies a slightly larger change in shell Mg/Ca per °C for *Uvigerina sp.* (Mg/Ca_{Uvi} = 0.87e0.15*T) which we apply directly in this study. *Martin et al.* [2002b] previously used the same equation adjusted to core top Mg/Ca values from core TR163-31P but our new data from core TR163-20B suggest that this probably led to underestimates of glacial cooling in the deep Pacific. Error in calculating absolute temperatures estimated from the global calibration exceeds 1.2°C. Systematic downcore variations, however, indicate that Mg/Ca can resolve much smaller changes in temperature at a single site (14).

3. Results

3.1. Deep Sea Temperatures Over the Last 90 kyr

[9] The warming accompanying deglaciation is recorded by both benthic foraminiferal Mg/Ca records presented here (Figure 2). Both records show similar trends of increasing Mg/Ca culminating in a maximum at the end of the deglaciation; however, higher Mg/Ca values in core TR163-20B over the latter half of the deglaciation imply a larger deep Pacific glacial-interglacial temperature change (Figure 2). Evidence in the core top calibration suggests that intense dissolution (or a fractionation effect during calcification related to saturation state) may lower the Mg/Ca of benthic foraminifera [*Martin et al.*, 2002a]. We suspect the Mg/Ca values in core TR163-31P over the latter half of the deglaciation and early Holocene may have been lowered by dissolution. If dissolution has led to lower Mg/Ca temperatures (and thus lower reconstructed temperatures) in the youngest section of TR163-31P, we might also expect that the values for the oldest 5–10 kyr of the record here (corresponding to MIS 5) underestimate absolute temperatures. Although the two cores are relatively close in geographic setting and water depth, TR163-31P is located much closer to the continental margin while TR163-20B is on the Galapagos platform; differences in the productivity of the overlying waters and the flux of remineralizable carbon to both sites could likely account for differences in dissolution intensity. Our most compelling evidence that TR163-20B is a better recorder of Holocene bottom water temperature is that applying the *Uvigerina sp.* calibration derived directly from the Atlantic yields a temperature for the core top close to the in situ bottom water temperatures in that region and a temperature estimate for the LGM comparable to estimates derived from pore water data [*Schrag et al.*, 1996]. In addition, the coldest temperatures derived using the new calibration yield temperatures only slightly lower than the freezing point of seawater and exceed freezing in only a few intervals. We also note the young age of core top planktonic foraminifera from TR163-20B relative to TR163-31B, the companion core to TR163-31P (1640 versus 5340 radiocarbon years) [*Brown and Elderfield*, 1996; *Dekens et al.*, 2002; *Le et al.*, 1995; *Levitus and Boyer*, 1994; *Martin et al.*, 2002b; *Rosenthal et al.*, 1997]. Despite the presence of this artifact, both records show a similar pattern of variance during the deglaciation. These new estimates of temperature change over the deglaciation are ~1°C larger than temperatures estimated from regional comparison of benthic $\delta^{18}O$ records [*Labeyrie et al.*, 1987] but comparable to estimates of deep sea cooling inferred from pore water $\delta^{18}O$ changes [*Adkins and Schrag*, 2001; *Schrag et al.*, 1996].

[10] Pacific deep water temperature over the last glacial (10–90 ka BP) correlates with Antarctic air temperature and atmospheric pCO_2 (Figure 3). Variability in benthic Mg/Ca

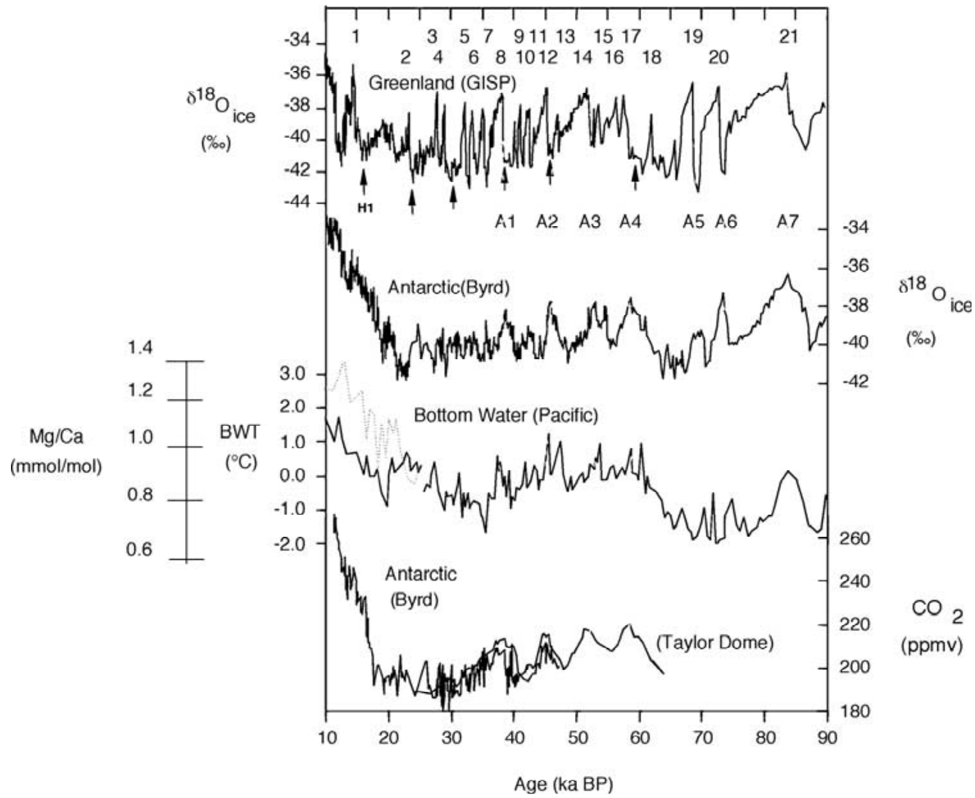

Figure 3. Comparison of benthic Mg/Ca from the deep eastern Pacific (a proxy for deep water temperatures changes) with climate records from Greenland and Antarctic ice cores [*Blunier and Brook*, 2001; *Grootes et al.*, 1993; *Indermuhle et al.*, 2000; *Johnsen et al.*, 1972]. The broad pattern of deep water temperature variations (Mg/Ca) over the last 90,000 years recorded in TR163-31P (solid line) and TR163-20B (dashed line) resembles changes in Antarctic air temperature recorded in the Byrd ice core ($\delta^{18}O$) and atmospheric CO_2 concentration recorded in Taylor Dome. There is clear millennial-scale variability in deep water temperature between 40 and 70 ka BP (corresponding to MIS 3) but the moderate accumulation rate (~8 cm/kyr) and minimal age-depth tie points for the deep sea sediment record prevent us from distinguishing whether the events are synchronous with events in Greenland or Antarctica. Figure modeled after *Blunier and Brook* [2001]. The ice core records from Byrd and GISP are on the published GISP2 timescale, correlated using the methane variations. The Taylor Dome CO_2 record has also been converted to the GISP2 timescale by correlating the published methane record for the core with the GISP methane record (see supplementary data) [*Indermuhle et al.*, 2000; *Brook*, 2000; *Brook et al.*, 1999; *Stuiver et al.*, 1988].

between 40 and 60 ka BP is consistent with instability identified in other components of the climate system during this period [*Curry and Oppo*, 1997; *Dansgaard et al.*, 1993; *Shackleton et al.*, 2000] and is direct evidence for millennial-scale oscillations in deep water temperature. Although it is not possible to distinguish whether the millennial-scale deep water temperature oscillations we observe in TR163-31P are in phase with Antarctic air temperatures (because of the moderate sedimentation rate at this site), [*Shackleton et al.* [2000] have observed millennial-scale $\delta^{18}O$ variability in a high sedimentation rate (~30 cm/kyr) deep Atlantic core that clearly correlates with air temperature variability over Antarctica. Whereas they attribute the variability to rapid variations in ice volume, a new analysis of millennial-scale sea-level changes deduced from coral terraces at Huon Peninsula suggests that deep-water temperature variability may be responsible for a significant fraction of ~0.5 per mil $\delta^{18}O$ variations [*Chappell*, 2002]. Together these records establish a temporal correlation between atmospheric CO_2 and the temperature of the deep sea over the last glacial cycle (Figures 3 and 4) and also provide independent estimates of temperature changes during MIS 3.

[11] Assuming the four small, millennial-scale oscillations in bottom water temperature and CO_2 between 40 and 65 ka (MIS 3) are correlative events yields a CO_2/T slope of approximately 12 μatm/°C (Figure 4). The amplitude of millennial-scale temperature events is more likely underestimated than overestimated. With a sedimentation rate of ~8 cm/kyr at the site of TR163-31P, the millennial-scale temperature changes may have been attenuated by ~40% or more which would imply larger temperature changes (and smaller CO_2/T sensitivity) [*Anderson*, 2001]. For the deglaciation, the slope depends on the estimate of temperature change: a 3–4°C warming from the LGM to early Holocene (Figures 2 and 3), consistent

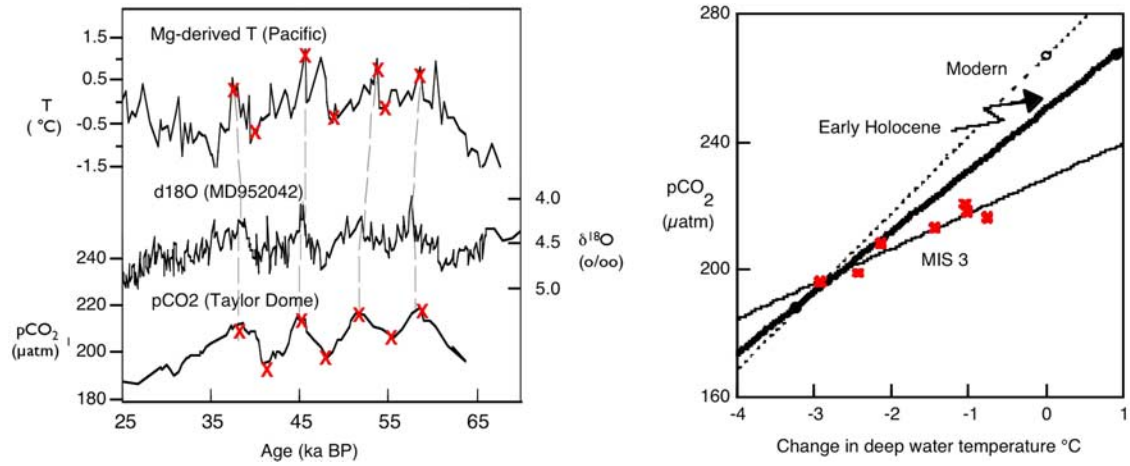

Figure 4. (left) Comparison of Mg-derived Pacific deep water temperatures, benthic $\delta^{18}O$ from the deep Atlantic, and record of atmospheric CO_2 recorded in Taylor Dome Antarctica. The benthic $\delta^{18}O$ events in the high accumulation rate (~30 cm/kyr) core MD952042 have been previously shown to correlate with suborbital events in Antarctic air temperature [*Shackleton et al.*, 2000]. Our Mg/Ca record suggests that a significant fraction of the benthic $\delta^{18}O$ variation reflects temperature. Red crosses mark points used to derive relations shown in right panel. (right) Data-derived relationship between atmospheric CO_2 recorded in Taylor Dome Antarctica [*Indermuhle et al.*, 2000] and bottom water temperature changes. We have defined sensitivities for MIS 3 and the deglaciation using the bottom water temperature records from TR163-31P (MIS 3) and TR163-20B (deglaciation). For MIS 3 the change in atmospheric CO_2 per °C (solid black line) is defined using maxima and minima in the bottom water temperature record assumed to be correlative with peaks and valleys in the Taylor Dome pCO_2 record (~12 µatm/°C). For the deglaciation the lower limit of the sensitivity in atmospheric CO_2 per °C (~17 µatm/°C) is defined using the early Holocene temperature maximum, whereas the upper limit (~26 µatm/°C) is defined assuming modern bottom water temperatures/core top values, defined in the figure as the "steady state" response. In both cases we ignore mismatches in timing (shown in Figure 2). The slope of the "deglaciation" line is comparable to the theoretical maximum steady state response, which is constrained, independent of the paleodata, by modern bottom water temperatures in the deep Pacific and the freezing point of seawater.

with new Mg/Ca data and pore water estimates, yields a slope of 17 or 26 µatm/°C. Using the lower estimates of Holocene temperature from core TR163-31P yields a slope of ~26–35 µatm/°C. Therefore, in either case, the paleodata indicate that the relationship between bottom water temperature changes and CO_2 for the deglaciation (26 ± 9 µatm/°C) is steeper than the value defined by the events in MIS 3 (~12 µatm/°C).

3.2. The pCO_2/T Relation Derived From Numerical Experiments

[12] For comparison with the paleodata, we evaluated the pCO_2 sensitivity to the mean temperature of the ocean through a series of ocean box and GCM carbon cycle model experiments (Figure 5) [*Shin et al.*, 2003; *Winguth et al.*, 2000]. The solubility of CO_2 in a homogeneous seawater solution increases by about 4%/°C decreasing temperature due to changes in the equilibrium constants for CO_2 solubility and pH reactions [*Chipman et al.*, 1992]. Linearized about a midpoint of glacial-interglacial pCO_2 change (~240 µatm/°C), this translates to a CO_2/T relation of ~10 µatm/°C. It is tempting to use changes in sea surface temperatures to estimate the glacial/interglacial solubility effect; however, previous modeling experiments have shown that the solubility cannot be estimated from a simple weighted average of surface waters. Instead, the steady state CO_2 concentration of the atmosphere is biased toward forcing in the high latitudes where deep waters form, an effect which is more pronounced in box models but still significant in general circulation models of the ocean carbon cycle [*Archer et al.*, 2000a; *Broecker et al.*, 1999].

[13] To assess the effect of only changing the solubility of CO_2 gas, we conducted two sets of numerical experiments. In the first set of experiments (labeled "Thermo" in Figure 5), we incrementally cooled mean ocean temperatures using a modern ocean circulation field. For simplicity, mean ocean temperature was changed in the "Thermo" GCM runs by uniformly changing surface water temperatures which led to a mean ocean temperature change. We experimented with incrementally lowering mean ocean temperature by independently lowering high-latitude and tropical sea surface temperatures using the Pandora 12-box model; we found a comparable pCO_2 change per °C mean ocean temperature change for each scenario. Although records of tropical sea surface temperature change appear to be consistent with the 1–2°C oscillations during MIS 3

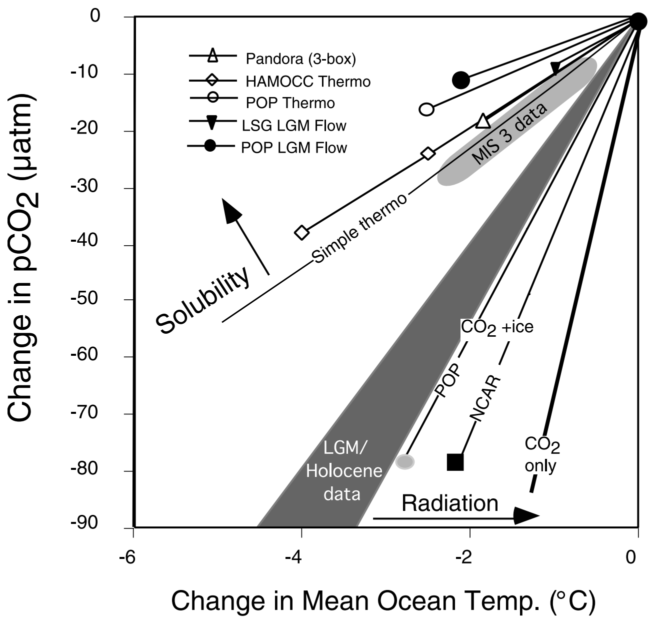

Figure 5. Model relationships between deep ocean temperature and the pCO_2 of the atmosphere. Solid line ("simple thermo") is the solubility of CO_2 gas into a homogeneous seawater solution, decreasing from 278 µatm. Pandora, HAMOCC Thermo, and POP (Los Alamos National Laboratory's Parallel Ocean Program) Thermo are new numerical experiments using global circulation carbon cycle models of the ocean, showing the effects of changing the solubility of the CO_2 gas only, with no changes in circulation or mixing of the ocean. LSG LGM and POP LGM are GCM results of changing the sea surface temperature forcing at the sea surface, which changes both CO_2 solubility and ocean circulation. These are all estimates of the solubility relation between CO_2 and deep sea temperature. "CO_2 only" is from the GFDL coupled climate model equilibrium run of doubled CO_2 described by Stouffer and Manabe [*Stouffer and Manabe*, 1999]. NCAR Greenhouse is from the NCAR CCSM coupled climate model runs described by *Shin et al.* [2003]. POP Greenhouse is the result of driving the POP ocean model using sea surface forcing from the *Shin et al.* [2003] simulation. These are both estimates of the radiative relation between CO_2 and deep sea temperature with CO_2 specified. Gray regions are estimates of the CO_2/deep ocean T relation derived from paleodata for stage 3 and for the deglaciation.

that we observe in the deep sea record [*Lea et al.*, 2001], this need not be the case to change pCO_2 through the solubility effect. Archer et al. previously demonstrated that the tropical sea surface temperatures are not an effective barrier to deep sea temperatures and have little direct effect on pCO_2 [*Archer et al.*, 2000b].

[14] In a second set of experiments, (labeled "LGM Flow") we allowed glacial temperature and climate forcing to drive the ocean circulation. Forcing for the large-scale geostrophic (LSG) general circulation model (GCM) was derived from CLIMAP sea surface temperatures and sea ice distributions and by an adjoint fit of sea surface salinity distribution to reproduce biochemical tracers $\delta^{13}C$ and Cd in deep sea $CaCO_3$. The Parallel Ocean Program (POP) primitive equation GCM was forced by sea surface temperature and salinities from a coupled atmosphere/ocean climate model forced by LGM pCO_2, orbital forcing, and land ice conditions. In spite of the complexities, all of the models, box models and GCMs alike, show a slighter lower sensitivity (smaller CO_2 change per °C) than the strict thermodynamic relation, in the range of 6–10 µatm/°C.

[15] Quantifying the change in deep ocean temperature resulting from radiative (greenhouse) forcing requires long integrations of coupled models of the atmosphere and ocean. A ~4000 year run of the GFDL coupled climate model predicts a mean ocean warming of 3.5°C in response to a doubling of CO_2, translating to ~75 µatm/°C (heavy dashed line, Figure 5) [*Stouffer and Manabe*, 1999]. This result may not apply to the deglaciation, however, because LGM cooling was greater than would be expected from CO_2 forcing alone, presumably because of the albedo of the continental ice sheets. Combined ice sheet, orbital, and CO_2 forcing in a coupled atmosphere/ocean model [*Shin et al.*, 2003] resulted in a decrease in ocean temperature of 2.8°C (for LGM conditions), to give ~28 µatm/°C [*Liu et al.*, 2002]. We also drove the POP ocean model (used in the experiments above) using sea surface forcing from the coupled simulation [*Shin et al.*, 2003], and found a decrease in mean temperature by 3.2°C, to give 25 µatm/°C. The salient conclusions from these modeling exercises are (1) that the CO_2/T relation from radiative equilibrium is higher than that for solubility, and (2) its magnitude depends on whether the effects of ice sheet albedo are included in the definition of CO_2 climate forcing.

4. Discussion

4.1. What Is Forcing the System?

[16] Several studies have noted a correlation between Antarctic air temperature and atmospheric CO_2, not only over the longer timescales of 100 kyr glacial cycles but also on the shorter millennial-scale characteristic of variability during the last glacial [*Cuffey and Vimeux*, 2001; *Indermuhle et al.*, 2000; *Petit et al.*, 1999; *Stauffer et al.*, 1998]. Our data extend this correlation to the temperature of the deep sea over the last glacial cycle (Figure 3). Comparison of the observed and modeled CO_2/deep ocean T relations, however, highlights a distinction between the deglaciation and stage 3 events. The data for the deglaciation lie close to the model-derived radiative equilibrium obtained by forcing CO_2 and allowing for changes in the extent of ice sheets (~30 µatm/°C; Figure 5). Some mechanism for changing the pCO_2 of the atmosphere over the deglaciation, such as a change in the biological pump or the pH of the ocean, is required. During stage 3, the ice sheet changes due to albedo forcing presumably remained nearly constant, and the radiative equilibrium CO_2/T relation should have been no less than the LGM climate sensitivity (~30 µatm/°C) and, more likely, closer to modern climate sensitivity (75 µatm/°C). The data are very close to the model-derived solubility relation of ~10 µatm/°C (Figure 4).

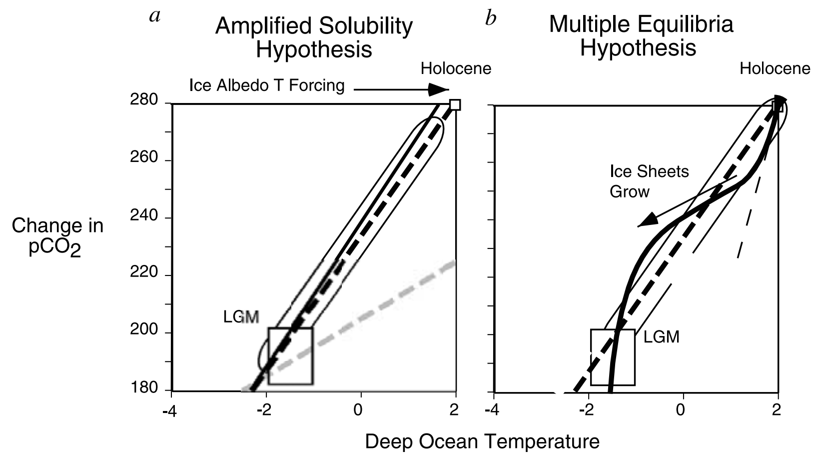

Figure 6. Schematic of the alternative scenarios for the interplay between the solubility and the radiative CO_2 relations during the LGM. The oval outlines the relation between CO_2 and temperature indicated by the paleodata. (a) Aspects of the climate system linked to temperature change, such as deep water formation and sea ice, could lead to larger changes in CO_2 effectively enhancing solubility. The gray dashed line is the solubility relation as shown in Figure 1. The combined effect of solubility and other mechanisms linked to temperature forcing shown by the black dashed line is the enhanced solubility relation. The enhanced solubility relation is steeper than the model derived solubility (gray dashed line) and nearly overlaps with the radiative relation (solid line, the same relation described in Figure 1). The similar slopes of the two relations would result in amplified feedback between CO_2 and temperature, making the system very sensitive to small perturbations. (b) Combining the effect of nonlinear ice albedo feedback with the radiative feedback would result in a system with multiple equilibria. The radiative relation is shown by the solid black curve. At CO_2 and ice volume near Holocene conditions, the relation is identical to the modeled radiative effect of for the CO_2-only scenario as shown in Figure 5; this is also shown by the thin dashed line. As temperature approaches freezing, further decreases in CO_2 cannot greatly reduce temperature thus there is a slope similar to the radiative relation at high CO_2/low ice volume. Connecting these extremes yields the radiative relation associated with large changes in ice volume. We use the enhanced solubility relation from Figure 6a (the thick gray dashed line). Intersections between the two relations define multiple equilibria.

CO_2 correlates with ocean temperature, but changes in temperature exceed what would be expected from radiative forcing alone. Apparently, over these 5-kyr events, externally forced changes in temperature drive pCO_2 according to the solubility of CO_2 in seawater.

[17] It is clear that the CO_2 changes from the effect of cooling on solubility itself cannot explain the amplitude of the LGM/Holocene CO_2 change. Given the remarkable linearity of CO_2 and T over the deglaciation [*Cuffey and Vimeux*, 2001; *Monnin et al.*, 2001], however, it is tempting to invoke an ‘‘enhanced’’CO_2 solubility effect. That is, we could infer that whatever mechanism pulls pCO_2 to low glacial levels responds causally to some aspect of glacial climate, generating a greater CO_2 sensitivity to temperature forcing than the solubility relation alone. Graphically, this could be envisioned as a change in the slope of the solubility response that yields a slope closer to the slope of the radiative response and amplifies the feedback (i.e., ‘enhanced solubility’; Figure 6a). It has been predicted, for example, that sea ice cover in the Southern Ocean might decrease atmospheric pCO_2 [*Stephens and Keeling*, 2000; *Morales Maqueda and Rahmstorf*, 2002; *Archer et al.*, 2003]. If sea ice extent responds to deep sea temperature [*Gildor and Tziperman*, 2001; *Keeling and Stephens*, 2001], then this mechanism could enhance the solubility CO_2 response to changing ocean temperature. Or, it could turn out that subpolar surface waters, which may undergo a larger temperature change than the global mean, control CO_2. Any form of CO_2 forcing (ocean pH or biological pump changes, for example) could contribute to an ‘‘enhanced solubility relation,’’ as long as it responds causally to glacial climate. Known CO_2 forcings during the deglaciation include uptake by the terrestrial biosphere and increased solubility due to dilution of ocean salinity by fresh meltwater. Taking these factors into account, we would require a solubility relation of 25–36 μatm/°C if we attribute the deglacial CO_2 rise to solubility alone. However, the solubility relation inferred from the stage 3 data is similar to our model derived value of 10 μatm/°C. Therefore, whichever mechanism is invoked for enhancing the solubility effect, it must be active only over orbital timescales, not over the shorter timescales.

[18] Similarly, considerations other than the direct effect of CO_2 changes the feedbacks between CO_2 and temperature. Ultimately, the effect of ice albedo responsible for much of the LGM cooling is not a forcing independent of CO_2, but must serve as an internal feedback, amplifying

the radiative equilibrium (Figure 6b) over times of ice volume change and possibly leading to multiple equilibria in the climate system. The amplified radiative relation must be a nonlinear one. Graphically, the combined effect could be represented by a change in the slope of the simply modeled radiative relation and its representation as a straight line (Figures 1 and 6a) that we construct as follows. At pCO_2 (and minimal ice volume) close to Holocene values the radiative relation is tangent to the climate model results of 60 μatm/°C (dashed thin line in Figure 6b), smoothly connecting to the global warming forecast. At LGM pCO_2, the temperature of the deep sea approaches freezing; constrained by freezing, the temperature becomes insensitive to further declines in pCO_2. These two regions of low temperature sensitivity, constrained respectively by low ice volume and low temperature, must be connected by an interval of higher sensitivity, corresponding to the growth of ice sheets (and the ice albedo feedback). If we couple this relation with an enhanced solubility mechanism as described above (the thick dashed line in Figure 6b), then the system will contain two stable equilibria at the intersections, one at low pCO_2 and one high. The only external forcing would be the thermal effect of orbital variations. Perhaps multiple equilibria of this type will ultimately explain the reproducibility of the glacial (200 μatm) and interglacial (280 μatm) pCO_2 values recorded in ice cores.

4.2. Mechanisms Driving Deep Sea Temperature Variations During MIS 3

[19] One potential mechanism to force the deep sea temperature is to alter the relative contributions of Antarctic Bottom Water (AABW) and North Atlantic Deep Water (NADW). The correlation between Antarctic air temperature [*Indermuhle et al.*, 2000] and deep water temperature suggests that the deep water warming events during MIS 3 may be linked to changes in deep water formation in the Southern Ocean. Modeling studies have demonstrated that overturning in the Southern Ocean is extremely sensitive to the density of surface waters, and that reduction in the export of a southern source bottom water leads to increased formation of North Atlantic Deep Water (NADW) [*Seidov et al.*, 2001]. Reduced density of surface waters may have arisen from changes in fresh water forcing. Alternatively, it is also possible that AABW actually warmed during the 5-kyr events. Paired records of Mg/Ca and $\delta^{18}O$ in planktonic foraminifera may help to distinguish between these hypotheses. However, in either case, an increase in the production of NADW relative to AABW would lead to warming of deep waters in the Atlantic and, presumably, an overall increase in mean ocean temperature.

[20] The fluctuations of deep ocean temperatures on short timescales during MIS 3 may play a role in the bipolar seesaw [*Stocker et al.*, 1992b], the climate oscillations between North and South high latitudes. The Greenland and Antarctic ice core temperature records correlated to each other using bubble methane concentrations [*Blunier and Brook*, 2001] reveal a remarkably consistent series of temperature cycles. Each cycle begins with a slow warming in Antarctica while Greenland remains cold or undergoes a series of increasingly cool Dansgaard-Oeschger (D-O) temperature oscillations. Then, Greenland temperature rises abruptly, after which both Antarctica and Greenland begin a slow cooling. If the temperature of the deep sea is coupled to temperature in Antarctica, then warming in the deep sea may ultimately trigger convection in the North Atlantic resulting in sudden warming in Greenland. Thus the bipolar seesaw may be the surface manifestation of a surface/deep process.

5. Summary

[21] Measurements of benthic foraminiferal Mg/Ca from the deep eastern tropical Pacific provide estimates of the amplitude of changes in mean ocean temperature during the last glacial period. The Mg/Ca data presented here imply mean ocean temperature changes of ~3–4°C over the deglaciation, slightly larger than our previous estimates [*Martin et al.*, 2002b] but consistent with recent estimates derived from pore water data [*Adkins and Schrag*, 2001; *Schrag et al.*, 1996]. The Mg data also reveal several repeated excursions of 1 to 2°C during marine isotope stage (MIS) 3 on the timescale of thousands of years. Comparison of the Mg-derived millennial-scale temperature changes with (1) previously published high resolution benthic foraminiferal $\delta^{18}O$ data, (2) estimates of sea-level changes from coral terraces ($\delta^{18}O_{water}$) and (3) Antarctic ice core records provide evidence of a temporal link between ocean temperature, Antarctic air temperature, and atmospheric CO_2 during the last glacial cycle.

[22] Quantitative estimates of the CO_2/T relation derived from the paleodata reveal two distinct slopes over the last 90,000 years, suggesting different mechanisms forced climate change on different timescales or during different climate states. Over the deglaciation, the paleodata show a large change in CO_2 per degree change in mean ocean temperature consistent with previous model-derived estimates of CO_2 forcing which account for the radiative effect of CO_2 as well as changes in ice albedo. In this case, we still require external forcing (changes in ocean biology or pH, for example) to explain the full glacial-interglacial CO_2 change. Over the ~5-kyr-long climate oscillations during the last glacial (MIS 3), however, the paleodata show a smaller change in CO_2 and per ° T (~12 μatm/°C). This smaller change in sensitivity is consistent with new ocean GCM CO_2 solubility results showing increases in atmospheric CO_2 resulting from temperature-dependent solubility. The mean ocean temperature change forcing atmospheric CO_2 during MIS 3 may have resulted from changes in the production of AABW, implying an active role of the Southern high latitudes in the climate oscillations and "bipolar seesaw" that operated during the last glacial.

[23] **Acknowledgments.** We thank E. Boyle, N. Shackleton, and J. Kennett for samples; N. Shackleton for isotope analyses in core TR163-31P and J. Kennett for isotope analyses in core TR163-20B; Ray Pierrehumbert for comments on earlier drafts; M. Kashgarian for radiocarbon dating; development engineer H. Berg for mass spectrometer maintenance; and Larry Pederson for handling as well careful reading of the manuscript as editor.

References

Adkins, J., and D. Schrag (2001), Pore fluid constraints on deep ocean temperature and salinity during the Last Glacial Maximum, *Geophys. Res. Lett.*, *28*, 771–774.

Anderson, D. (2001), Attenuation of millennial-scale events by bioturbation in marine sediments, *Paleoceanography*, *16*, 352–357.

Archer, D. E., and E. Maier-Reimer (1994), Effect of deep-sea sedimentary calcite preservation on atmospheric CO_2 concentration, *Nature*, *367*, 260–264.

Archer, D. E., P. A. Martin, J. Milovich, V. Brovkin, G. Plattner, and C. Ashendel (2003), Model sensitivity in the effect of Antarctic sea ice and stratification on atmospheric pCO_2, *Paleoceanography*, *18*(1), 1012, doi:10.1029/2002PA000760.

Archer, D. E., G. Eshel, A. Winguth, W. S. Broecker, R. T. Pierrehumbert, M. Tobis, and R. Jacob (2000a), Atmospheric pCO2 sensitivity to the biological pump in the ocean, *Global Biogeochem. Cycles*, *14*, 1219–1230.

Archer, D. E., A. Winguth, D. W. Lea, and N. Mahowald (2000b), What caused the glacial/interglacial atmospheric p CO_2 cycles?, *Rev. Geophys.*, *38*, 159–189.

Berger, W. H. (1978), Sedimentation of deep-sea carbonate: Maps and models of variations and fluctuations, *J. Foraminiferal Res.*, *8*, 286–302.

Blunier, T., and E. J. Brook (2001), Timing of millennial-scale climate change in Antarctica and Greenland during the last glacial period, *Science*, *291*, 109–112.

Boyle, E. A., and L. D. Keigwin (1985), Comparison of Atlantic and Pacific paleochemical records for the last 215,000 years: Changes in deep ocean circulation and chemical inventories, *Earth Planet. Sci. Lett.*, *76*, 135–150.

Broecker, W., J. Lynch-Steiglitz, D. Archer, M. Hofmann, E. Maier-Reimer, O. Marchal, T. Stocker, and N. Gruber (1999), How strong is the Harvardton-Bear constraint?, *Global Biogeochem. Cycles*, *13*, 817–821.

Brook, E. J. (2000), On the origin and timing of rapid changes in atmospheric methane during the last glacial period, *Global Biogeochem. Cycles*, *14*, 559–572.

Brook, E. J., S. Harder, J. Severinghaus, and M. Bender (1999), Atmospheric methane and millennial-scale climate change, in *Mechanisms of Global Climate Change at Millennial Time Scales*, *Geophys. Monogr. Ser.*, vol. 112, edited by P. U. Clark, R. S. Webb, and L. D. Keigwin, pp. 165–175, AGU, Washington, D. C.

Brown, S., and H. Elderfield (1996), Variations in Mg/Ca and Sr/Ca ratios of planktonic foraminifera caused by postdepositional dissolution: Evidence of shallow Mg-dependent dissolution, *Paleoceanography*, *11*, 543–551.

Chappell, J. (2002), Sea level changes forced ice breakouts in the Last Glacial cycle: New results from coral terraces, *Quat. Res. Rev.*, *21*, 1229–1240.

Chappell, J., and N. J. Shackleton (1986), Oxygen isotopes and sea level, *Nature*, *324*, 137–140.

Chipman, D. W., J. Marra, and T. Takahashi (1992), Primary production at 47N and 20W in the North Atlantic Ocean: A comparison between the ^{14}C incubation method and mixed layer carbon budget observations, *Deep Sea Res.*, *40*, 151–170.

Cuffey, K. M., and F. Vimeux (2001), Covariation of carbon dioxide and temperature from the Vostok ice core after deuterium-excess correction, *Nature*, *412*, 523–526.

Curry, W. B., and D. W. Oppo (1997), Synchronous, high-frequency oscillations in tropical sea surface temperatures and North Atlantic Deep Water production during the last glacial cycle, *Paleoceanography*, *12*, 1–14.

Dansgaard, W., S. J. Johnsen, H. B. Clausen, D. Dahl-Jensen, N. S. Gundestrup, C. U. Hammer, C. S. Hvidberg, J. P. Steffensen, A. E. Sveinbjörnsdottir, J. Jouzel, and F. Bond (1993), Evidence for general instability of past climate from a 250-kyr ice-core record, *Nature*, *364*, 218–220.

Dekens, P. S., D. W. Lea, D. K. Pak, and H. J. Spero (2002), Core top calibration of Mg/Ca in tropical foraminifera: Refining paleotemperature estimation, *Geochem. Geophys. Geosyst.*, *3*(4), 1022, doi:10.1029/2001GC000200.

Gildor, H., and E. Tziperman (2001), Physical mechanisms behind biogeochemical glacial-interglacial CO_2 variations, *Geophys. Res. Lett.*, *28*, 2421–2424.

Grootes, P. M., M. Stuiver, J. W. C. White, S. J. Johnsen, and J. Jouzel (1993), Comparison of oxygen-isotope records from the GISP2 and GRIP Greenland ice cores, *Nature*, *366*, 552–554.

Indermuhle, A., E. Monnin, B. Stauffer, T. F. Stocker, and M. Wahlen (2000), Atmospheric CO_2 concentration from 60 to 20 kyr BP from the Taylor Dome ice core, Antarctica, *Geophys. Res. Lett.*, *27*, 735–738.

Johnsen, S. J., H. B. Dansgaard, H. B. Clausen, and C. C. Langway (1972), Oxygen isotope profiles through the Antarctic and Greenland ice sheets, *Nature*, *235*, 429–434.

Keeling, R. F., and B. B. Stephens (2001), Antarctic sea ice and the control of Pleistocene climate instability, *Paleoceanography*, *16*, 112–113.

Labeyrie, L. D., J. C. Duplessy, and P. L. Blanc (1987), Variations in mode of formation and temperature of oceanic deep waters over the past 12,5000 years, *Nature*, *327*, 477–482.

Le, J., et al. (1995), Late Quaternary paleoceanography in the eastern equatorial Pacific from planktonic foraminifers: A high-resolution record from Site 846, *Proc. Ocean Drill. Program Sci. Results*, *138*, 675–693.

Lea, D. W., D. Pak, and H. J. Spero (2001), Climate impact of late Quaternary equatorial Pacific sea surface temperature variations, *Science*, *289*, 1719–1724.

Lear, C. H., H. Elderfield, and P. A. Wilson (2000), Cenozoic deep-sea temperatures and global ice volumes from Mg/Ca in benthic foraminiferal calcite, *Science*, *287*, 269–272.

Levitus, S., and T. P. Boyer (1994), *World Ocean Atlas 1994*, vol. 4, *Temperature*, U.S. Dept. of Comm., Washington, D. C.

Liu, Z., S. Shin, B. Otto-Bliesner, J. E. Kutzbach, E. C. Brady, and D. Lee (2002), Tropical cooling at the last glacial maximum and extratropical ocean ventilation, *Geophys. Res. Lett.*, *29*(10), 1409, doi:10.1029/2001GL013938.

Manabe, S., and A. J. Broccoli (1985), The influence of continental ice sheets on the climate of an ice age, *J. Geophys. Res.*, *90*, 2167–2190.

Martin, P. A., and D. W. Lea (2002), A simple evaluation of cleaning procedures on fossil benthic foraminiferal Mg/Ca, *Geochem. Geophys. Geosyst.*, *3*(10), 8401, doi:10.1029/2001GC000280.

Martin, P. A., D. W. Lea, and D. C. McCorkle (2002a), Examining the evidence for the influence of carbonate saturation state on benthic foraminiferal Mg/Ca, *Eos Trans. AGU*, *83*(47), Fall Meet. Suppl., Abstract PP52B-12.

Martin, P. A., D. W. Lea, Y. Rosenthal, N. J. Shackleton, M. Sarthein, and T. Papenfuss (2002b), Quaternary deep sea temperature histories derived from benthic foraminiferal Mg/Ca, *Earth Planet. Sci. Lett.*, *198*, 193–209.

Milankovitch, M. (1930), *Mathematische Klimalehre und Astronomishe Theorie der Klimaschwankungen*, 176 pp., Gebruder Borntreger, Berlin.

Monnin, C., A. Indermuhle, A. Dallenbach, J. Fluckiger, B. Stauffer, T. F. Stocker, D. Raynaud, and J.-M. Barnola (2001), Atmospheric CO_2 Concentrations over the Last Glacial Termination, *Science*, *291*, 112–114.

Morales Maqueda, M. A., and S. Rahmstorf (2002), Did Antarctic sea-ice expansion cause glacial CO_2 decline?, *Geophys. Res. Lett.*, *29*(1), 1011, doi:10.1029/2001GL013240.

Petit, J. R., et al. (1999), Climate and atmospheric history of the past 420,000 years from the Vostok ice core, Antarctica, *Nature*, *399*, 429–436.

Rosenthal, Y., E. A. Boyle, and N. Slowey (1997), Temperature control on the incorporation of magnesium, strontium, fluorine, and cadmium into benthic foraminiferal shells from Little Bahama Bank: Prospects for thermocline paleoceanography, *Geochim. Cosmochim. Acta*, *61*, 3633–3643.

Rosenthal, Y., G. P. Lohmann, K. C. Lohmann, and R. M. Sherrell (2000), Incorporation and preservation of Mg in *Globigerinoides sacculifer* implications for reconstructing the temperature and $^{18}O/^{16}O$ of seawater, *Paleoceanography*, *15*, 135–145.

Schrag, D. P., G. Hampt, and D. W. Murray (1996), Pore fluid constraints on the temperature and oxygen isotopic composition of the glacial ocean, *Science*, *272*, 1930–1932.

Seidov, D., B. J. Haupt, E. J. Barron, and M. Maslin (2001), Ocean bi-polar seesaw and climate: Southern versus northern meltwater impacts, in *The Oceans and Rapid Climate Change: Past, Present and Future*, edited by D. Seidov, B. J. Haupt, and M. Maslin, pp. 147–167, AGU, Washington, D. C.

Shackleton, N. J. (2000), The 100,000-year ice-age cycle identified and found to lag temperature, carbon dioxide, and orbital eccentricity, *Science*, *289*, 1897–1902.

Shackleton, N. J., M. A. Hall, and E. Vincent (2000), Phase relationships between millennial-scale events 64,000–24,000 years ago, *Paleoceanography*, *15*, 565–569.

Shin, S.-I., Z. Liu, B. Otto-Bliesner, E. C. Brady, J. E. Kutzbach, and S. P. Harrison (2003), A simulation of the Last Glacial Maximum using the NCAR-CCSM, *Clim. Dyn.*, *20*, 127–151.

Stauffer, B., et al. (1998), Atmospheric CO_2 concentration and millennial-scale climate change during the last glacial period, *Nature*, *392*, 59–62.

Stephens, B. B., and R. F. Keeling (2000), The influence of Antarctic sea ice on glacial-interglacial CO_2 variations, *Nature*, *404*, 171–174.

Stocker, T. F., D. G. Wright, and W. S. Broecker (1992a), The influence of high-latitude surface forcing on the global thermohaline circulation, *Paleoceanography*, *7*, 529–542.

Stocker, T. F., D. G. Wright, and L. A. Mysak (1992b), A zonally averaged, coupled ocean-atmosphere model for paleoclimatic studies, *J. Clim.*, *5*, 773–797.

Stouffer, R. J., and S. Manabe (1999), Response of a coupled ocean-atmosphere model to increasing atmospheric carbon dioxide: Sensitivity to the rate of increase, *J. Clim.*, *12*, 2224–2237.

Stuiver, M., P. J. Reimer, E. Bard, J. W. Beck, G. S. Burr, K. A. Jughen, B. Kromer, F. G. McCormac, J. Plicht, and M. Spurk (1988), NTCAL98 radiocarbon age calibration, 24,000–0 cal BP, *Radiocarbon*, *40*, 1041–1083.

Volk, T., and M. I. Hoffert (1985), Ocean carbon pumps: Analysis of relative strengths and efficiencies in ocean-driven atmospheric CO_2 changes, in *The Carbon Cycle and Atmospheric CO_2: Natural Variations Archean to Present*, *Geophys. Res. Lett.*, vol. 32, edited by E. T. Sundquist, pp. 99–110, AGU, Washington, D. C.

Winguth, A., D. Archer, E. Maier-Reimer, and U. Mikolajewicz (2000), Paleonutrient data analysis of the glacial Atlantic using an adjoint ocean general circulation model, in *Inverse Methods in Global Biogeochemical Cycles*, *Geophys. Res. Lett.*, vol. 114, edited by P. Kasibhatla et al., pp. 171–183, AGU, Washington, D. C.

D. Archer and P. Martin, Department of Geophysical Sciences, University of Chicago, Chicago, IL 60637, USA. (pmartin@uchicago.edu)

D. W. Lea, Department of Geological Sciences and the Marine Sciences Institute, University of California at Santa Barbara, Santa Barbara, CA 93106, USA.